Agricultural and Forest Meteorology 275 (2019) 47–58

Contents lists available at ScienceDirect

Agricultural and Forest Meteorology

journal homepage: www.elsevier.com/locate/agrformet

Negative extreme events in gross primary productivity and their drivers in China during the past three decades

Weizhe Chen[a,b], Dan Zhu[b], Chunju Huang[a,c,*], Philippe Ciais[b], Yitong Yao[d], Pierre Friedlingstein[e], Stephen Sitch[f], Vanessa Haverd[g], Atul K. Jain[h], Etsushi Kato[i], Markus Kautz[j], Sebastian Lienert[k], Danica Lombardozzi[l], Benjamin Poulter[m], Hanqin Tian[n], Nicolas Vuichard[b], Anthony P. Walker[o], Ning Zeng[p]

[a] State Key Laboratory of Biogeology and Environmental Geology, School of Earth Sciences, China University of Geosciences, Wuhan 430074, China
[b] Laboratoire des Sciences du Climat et de l'Environnement, LSCE/IPSL, CEA-CNRS-UVSQ, Université Paris-Saclay, Gif-sur-Yvette, 91191, France
[c] Hubei Key Laboratory of Critical Zone Evolution, School of Earth Sciences, China University of Geosciences, Wuhan 430074, China
[d] Sino-French Institute for Earth System Science, College of Urban and Environmental Sciences, Peking University, Beijing 100871, China
[e] College of Engineering, Mathematics and Physical Sciences, University of Exeter, Exeter EX4 4QF, UK
[f] College of Life and Environmental Sciences, University of Exeter, Exeter EX4 4RJ, UK
[g] CSIRO Oceans and Atmosphere, Canberra 2601, Australia
[h] Department of Atmospheric Sciences, University of Illinois, Urbana, IL 61801, USA
[i] Institute of Applied Energy (IAE), Minato, Tokyo 105-0003, Japan
[j] Forest Research Institute Baden-Württemberg, Freiburg 79100, Germany
[k] Climate and Environmental Physics, Physics Institute and Oeschger Centre for Climate Change Research, University of Bern, Bern CH-3012, Switzerland
[l] Climate and Global Dynamics Division, National Center for Atmospheric Research, Boulder, CO 80302, USA
[m] NASA Goddard Space Flight Center, Biospheric Science Laboratory, Greenbelt, MD 20771, USA
[n] International Center for Climate and Global Change Research, School of Forestry and Wildlife Sciences, Auburn University, 602 Duncan Drive, Auburn, AL 36849, USA
[o] Environmental Sciences Division & Climate Change Science Institute, Oak Ridge National Laboratory, Oak Ridge, TN 37831, USA
[p] Department of Atmospheric and Oceanic Science, University of Maryland, College Park, MD 20742-2425, USA

ARTICLE INFO

Keywords:
Climate change
Extreme events
Gross primary production
Power law distribution
China

ABSTRACT

Climate extremes have remarkable impacts on ecosystems and are expected to increase with future global warming. However, only few studies have focused on the ecological extreme events and their drivers in China. In this study, we carried out an analysis of negative extreme events in gross primary productivity (GPP) in China and the sub-regions during 1982–2015, using monthly GPP simulated by 12 process-based models (TRENDYv6) and an observation-based model (Yao-GPP). Extremes were defined as the negative 5th percentile of GPP anomalies, which were further merged into individual extreme events using a three-dimensional contiguous algorithm. Spatio-temporal patterns of negative GPP anomalies were analyzed by taking the 1000 largest extreme events into consideration. Results showed that the effects of extreme events decreased annual GPP by 2.8% (i.e. 208 TgC $year^{-1}$) in TRENDY models and 2.3% (i.e. 151 TgC $year^{-1}$) in Yao-GPP. Hotspots of extreme GPP deficits were mainly observed in North China (-53 gC m^{-2} $year^{-1}$) in TRENDY models and Northeast China (-42 gC m^{-2} $year^{-1}$) in Yao-GPP. For China as a whole, attribution analyses suggested that extreme low precipitation was associated with 40%–50% of extreme negative GPP events. Most events in northern and western China could be explained by meteorological droughts (i.e. low precipitation) while GPP extreme events in southern China were more associated with temperature extremes, in particular with cold spells. GPP was revealed to be much more sensitive to heat/drought than to cold/wet extreme events. Combined with projected changes in climate extremes in China, GPP negative anomalies caused by drought events in northern China and by temperature extremes in southern China might be more prominent in the future.

* Corresponding author at: State Key Laboratory of Biogeology and Environmental Geology, School of Earth Sciences, China University of Geosciences, Wuhan 430074, China.
E-mail address: huangcj@cug.edu.cn (C. Huang).

https://doi.org/10.1016/j.agrformet.2019.05.002
Received 5 September 2018; Received in revised form 19 April 2019; Accepted 4 May 2019

1. Introduction

Gross primary productivity (GPP) is the largest carbon flux, changes of which affect the whole terrestrial carbon cycle. The CO_2 fertilization and growing season extension are expected to enhance vegetation growth and increase terrestrial net primary productivity (Los, 2013; Piao et al., 2013; Zhu et al., 2016). However, at the same time, it has been suggested that climate extremes may alter the composition, structure and function of ecosystems and therefore have potential negative impacts on terrestrial carbon uptake (Du et al., 2018; von Buttlar et al., 2018). For instance, the 2003 extreme heat wave and drought in Europe caused up to 30% reduction in GPP and resulted in a strong anomalous net source of CO_2 (Ciais et al., 2005). Based on the commonly used definition of climate extremes, IPCC (2012) pointed out that changing climate has led to changes in the frequency, intensity, spatial extent, duration, and timing of weather and climate extremes, and can result in unprecedented impacts on terrestrial carbon cycle. Furthermore, climate change is projected to further increase the frequency, persistence and intensity of climate extremes in the mid- to late 21 st century because of the on-going global warming (IPCC, 2013; Niu et al., 2017; Sui et al., 2018), which makes the impacts of future climate change on terrestrial ecosystem more uncertain (Samaniego et al., 2018; Yao et al., 2019). Therefore, characterizing climatic extreme events and their consequences on ecosystems is an important step for the development of adaptation strategies and risk reduction in the context of future climate change.

Extreme events are generally defined as statistically unusual episodes or occurrences, which are beyond the bounds of typical or normal variability (Reichstein et al., 2013). In scientific literature, extreme events have been defined in several ways—both from climatic and impact perspectives (Felton and Smith, 2017). Lloyd-Hughes (2012) firstly proposed a novel 3-dimensional (longitude, latitude, time) structure-based approach to describe drought events. Zscheischler et al. (2013) further improved the method and performed the first global analysis of spatio-temporally contiguous carbon-cycle extremes. This method has advantages in analyzing the size, shape, temporal evolution and other interesting quantities of extreme events. By using this technique, Zscheischler et al. (2014a) demonstrated that the largest 1000 negative GPP extremes accounted for a decrease in global photosynthetic carbon uptake of approximately 3.5 PgC $year^{-1}$, with most events being attributable to water scarcity. Huang et al. (2016) quantified sensitivities of GPP to spatio-temporally contiguous hydrological extreme events and implied that vegetation in Earth System Models (ESMs) was on average more sensitive to droughts than observed. Model output of the Coupled Model Intercomparison Project Phase 5 (CMIP5) future projections suggested that negative extremes in GPP would be driven by concurrent dry and hot conditions during the 21 st century (Zscheischler et al., 2014d). Zscheischler et al. (2018) pointed out that traditional assessment methods which considered only one driver at a time underestimated risk from extreme events, highlighting a better understanding of compound events.

The negative impacts of climate extremes on natural ecosystems and agriculture have been widely reported in China. Yuan et al. (2016) found that the 100-year return heat wave and drought in the summer of 2013 in southern China significantly reduced regional GPP, and produced the largest negative crop yield anomaly since 1960. The anomalous 2008 ice storm episode resulted in increased vegetation mortality, which exceeded recruitment for evergreen and deciduous broad-leaved species in central China (Ge et al., 2015). The most severe spring drought over the last five decades in 2010 in southwestern China reduced regional annual GPP by 4%, producing the lowest annual GPP over the period 2000–2010 (Zhang et al., 2012). Dynamic Land Ecosystem Model-based analysis showed that drought stress led to a large reduction of crop yield in China (Ren et al., 2012), with the maximum reduction in crop yield (−17.5%) occurred in 2000, a year with extreme drought and relatively high O_3 concentrations (Tian et al., 2016). The temperature and precipitation anomalies were the principal drivers of Normalized Difference Vegetation Index (NDVI) variation in the Yangtze River Basin (YRB) in recent years (Cui et al., 2018). These regional studies or case studies improved our understanding of the vulnerability and response of terrestrial ecosystems to individual extreme climate events. Nevertheless, most previous studies in China mainly focus on either the impacts of climate extremes (Chen et al., 2018; Yao et al., 2018a; Yuan et al., 2016) or only a few cases of ecological extreme events (Yuan et al., 2016; Zhang et al., 2012) but did not analyze a large number of extreme events in GPP in a systematic approach.

The sensitivity and vulnerability of ecosystem productivity to climate variability are expected to vary widely in different ecosystems and different climate zones, affected also by biodiversity or management practices (Isbell et al., 2015; Wang et al., 2017; Yao et al., 2018b; Zhou et al., 2015). China has different climate zones that range from tropic in the south to subarctic zone in the north, comprising wide ranges of precipitation and temperature gradients. However, there are a limited number of studies on the effects of multiple climate drivers on GPP in China. Thus, we intend to provide a statistical analysis of extreme events in GPP and their drivers at the national scale and the nine subregions (Fig. 1a). This study aims to (1) diagnose the spatial and temporal patterns of extreme events in GPP in China; (2) evaluate the response of GPP to extreme climatic drivers; (3) explore size distribution of GPP extreme events for different climate drivers and different regions. We expect to provide a better understanding of the characteristics of GPP extreme events and their responses to different drivers.

2. Materials and methods

2.1. GPP data sources

Results from an observation-based model of GPP (Yao-GPP, hereafter and Table 1), with 0.1° spatial resolution and monthly temporal frequency over China, were obtained from Yao et al. (2018b). The GPP data were developed using a machine learning technique, model tree ensembles (MTE) (Jung et al., 2011) with eddy flux measurements from 40 sites in China and the surrounding countries. The high-resolution GPP data can successfully capture the spatio-temporal variations of the GPP observed at the flux sites, including validation flux sites that were not part of the MTE training set (Yao et al., 2018b).

Besides the above observation-based model, we also used monthly GPP from process-based ecosystem models that took part in the historical climate carbon cycle model intercomparison project (TRENDYv6, Table A.1). The model simulations all followed the same experimental protocol (Le Quéré et al., 2018; Sitch et al., 2015) and were driven with the same climate data from the Climatic Research Unit and National Center for Environmental Prediction (CRU-NCEP) climate forcing reconstruction. The GPP outputs were from the S3 TRENDY simulations which used observed CO_2 concentrations, changing climate, and land cover changes as forcing over the period 1860–2016. Many different process-based models were used in TRENDY simulations. As coarse spatial resolution makes it not possible to diagnose enough GPP extreme events, model simulations with coarser resolution than 1° were excluded. Consequently, 12 models were finally selected: CABLE (Haverd et al., 2018), CLM4.5 (Oleson et al., 2013), DLEM (Tian et al., 2015), ISAM (Jain et al., 2013), LPJ-GUESS (Smith et al., 2014), LPJ-wsl (Sitch et al., 2003), LPX-Bern (Keller et al., 2017), ORCHIDEE (Krinner et al., 2005), ORCHIDEE-MICT (Guimberteau et al., 2018), SDGVM (Woodward et al., 1995), VEGAS (Zeng et al., 2005) and VISIT (Kato et al., 2013), and see references and further model details contained in Le Quéré et al. (2018).

2.2. Climatic data

To attribute negative extreme events in GPP to drivers, we used air

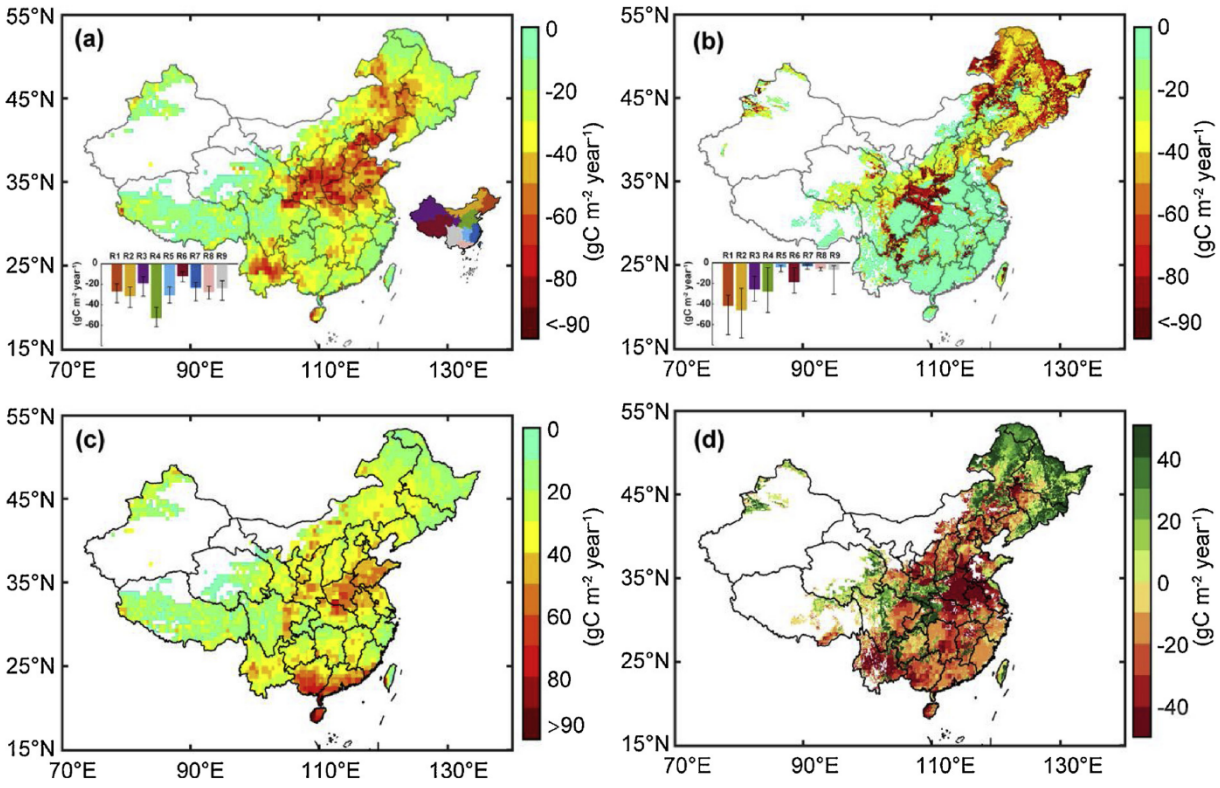

Fig. 1. Spatial distributions of (a) the magnitude of the 1000 largest negative extreme events in GPP (GPP_{1000}) during 1982–2015 from the median of the 12 process-based TRENDY models and (b) the observation-based GPP model Yao-GPP, (c) standard deviation over TRENDY models and (d) the TRENDY median minus Yao-GPP (i.e. panel (a) minus panel (b)). The left insets in panel (a) and (b) denote the median (i.e. bar graph), 25th and 75th percentile (i.e. error bar) of GPP anomalies for each sub-region. The right inset in panel (a) presents the definition of the nine sub-regions in China. R1 (red): Northeast China; R2 (orange): Inner Mongolia; R3 (purple): Northwest China; R4 (green): North China; R5 (sky blue): Central China; R6 (dark red): Qinghai-Tibetan Plateau (QTP); R7 (dark blue): Southeast China; R8 (pink): South China, and R9 (grey): Southwest China.

temperature (T), precipitation (P), soil moisture (SM), self-calibrating Palmer Drought Severity Index (scPDSI) (van der Schrier et al., 2013), burned area (BA) and CO_2 emissions from fires (FE) (Table 1). Gridded T and P data (0.5° spatial resolution) was taken from the monthly dataset compiled by the CRU of the University of East Anglia, UK. This CRU datasets span the period 1901–2015 and can be obtained at http://www.cru.uea.ac.uk/data. As Yao-GPP was driven by another forcing dataset, which was developed by Data Assimilation and Modeling Center for Tibetan Multi-spheres, Institute of Tibetan Plateau Research, Chinese Academy of Sciences (ITPCAS, http://westdc.westgis.ac.cn), the corresponding monthly T and P (Fig. A.1) were used to identify the driving factors for Yao-GPP. We used the respective SM data from TRENDY models to diagnose the contribution of SM to their GPP extremes. As for Yao-GPP, averaged TRENDY SM was used in attribution analysis. The scPDSI data, which represents an index for comparing the relative spatio-temporal variability of soil moisture changes over wide regions, was also collected from CRU. The Global Fire Emissions Database, Version 4 (GFEDv4) provides global estimates of monthly burned area and carbon emissions from fire (https://daac.ornl.gov/VEGETATION/guides/fire_emissions_v4.html). The data have a 0.25° spatial resolution and is available from July 1997 through 2015.

2.3. Preprocessing method

All of the gridded datasets were first resampled to 0.1° × 0.1° spatial resolution using the nearest neighbor interpolation. The original GPP and climate variables contain long-term trends and strong seasonal cycles. For these variables (i.e. T, P, scPDSI, SM and all the GPP data), the temporal linear trend and mean seasonal cycle were removed in each grid cell to get the anomalies of the time series data. For the variables describing episodic events (BA and FE), we divided them by the total sum of the respective time series in each grid cell. The

Table 1
Summary of monthly GPP estimates, climate and fire data used in this study. Some of the datasets extend beyond 1982–2015, but the analysis in this paper is confined to those years.

Data source	Variable	Resolution	Period	Citation
Yao-GPP	GPP	0.1°	1982-2015	Yao et al. (2018b)
Historical climate carbon cycle model intercomparison project (TRENDYv6)	GPP and soil moisture	0.5°-1°	1982-2015	Le Quéré et al. (2018)
Institute of Tibetan Plateau Research, Chinese Academy of Sciences (ITPCAS)	Air temperature and precipitation	0.1°	1982-2015	Chen et al. (2011)
Climatic Research Unit (CRU)	Air temperature and precipitation	0.5°	1982-2015	Harris et al. (2014)
Climatic Research Unit (CRU)	self-calibrating Palmer Drought Severity Index	0.5°	1982-2015	van der Schrier et al. (2013)
Global Fire Emissions Database, Version 4 (GFEDv4)	Burned area and fire emissions	0.25°	1997-2015	Randerson et al. (2017)

preprocessing produced anomalies in de-trended GPP and climate, which represents deviations from the mean behavior (Zscheischler et al., 2013).

2.4. Negative extreme events detection

In scientific literature, extremes are usually defined based on either the probability of occurrence of given quantities or threshold exceedances (IPCC, 2012). In order to quantify the GPP extreme events, we defined extremes as the negative 5th percentile of all the GPP anomalies (derived from the above-mentioned preprocessing). Contiguous extreme negative GPP anomalies (i.e. voxels) are further merged into individual extreme events following Zscheischler et al. (2014a). By "contiguous", we mean any of the 26 neighbors in three-dimensional (latitude × longitude × time) space also experiencing an extreme GPP anomaly. The size of an extreme event is the summation of GPP anomalies over the spatio-temporal domain of the event cluster. With this algorithm, each GPP dataset produced 1000˜5000 extreme events for the whole China during the study period. As we are more interested in large events and hope to compare between models, we investigated the 1000 largest negative extreme events in GPP (GPP_{1000}) for the whole China and the 100 largest extreme events for each of the nine sub-regions.

2.5. Power laws identification

Power laws in frequency or size distributions were previously detected in a variety of natural phenomena (Clauset et al., 2009), such as global fire size distributions (Hantson et al., 2015) as well as intensities of earthquakes. In this study, we analyzed the size distribution of GPP extreme events for different climate drivers and different regions in China. According to Zscheischler et al. (2013), the size distribution of extreme events (s_e) can also be well approximated by a power law relationship as follows:

$$p(s_e) \sim s_e^{-\alpha} \quad (1)$$

where α is a constant parameter of the distribution known as the exponent or scaling parameter. The exponent α of the size distribution was diagnosed using the fitting technique of maximum likelihood presented by Clauset et al. (2009) (see http://tuvalu.santafe.edu/~aaronc/powerlaws/). This algorithm has been widely applied in diagnosing power law distributions in empirical data (Scannell et al., 2016). The α-value from the power-law function provides information on asymmetry in the size distribution of extreme events, indicating the relative number of extreme events of different sizes. An increase in α suggests an increasing proportion of small extreme events relative to large ones. It can also be used as an index to investigate the different patterns in extreme events for different drivers and regions. Clauset's method provides a goodness-of-fit parameter p-value, where p-value ≥ 0.1 indicates a good fit.

2.6. Attribution of negative extreme events

In order to identify possible drivers of individual negative extreme events in GPP, we adopted the attribution method from Zscheischler et al. (2013). For each event, we calculate the median of driver variable anomalies over the spatio-temporal domain of the event, which directly represents the anomaly intensity of the corresponding driver during the event. Then, we let the event shift in each time step and obtain a series of medians (M_s) as a function of time. As there are possibly lagged responses of ecosystems to all these drivers (Reichstein et al., 2013), we consider time lags of a maximum of three months. Then, if any of the medians within three months preceding the events is less (higher) than the 10th (90th) percentile of M_s, the driver (e.g. a cold spell or heat wave) is selected as influential for that event. An GPP extreme event is attributed to fire if either BA or CO_2 emissions from fires during the event is higher than 90th percentile. A single event is possible to be explained by multiple drivers. The attribution rate is defined as the proportion of studied events, which are attributed to any of the nine drivers (i.e. for all drivers) or a typical driver (e.g. for cold spell).

2.7. GPP sensitivity during the extreme events

We explored GPP sensitivity of different models to precipitation or temperature anomalies (i.e. heat wave, cold spell, drought and wet). For each model, the single driver-induced GPP extreme events were selected in order to extract the impact of this driver from potential additive effects. Then, we divided the mean GPP anomalies by mean precipitation or temperature anomalies over the voxels during the selected extreme events. For example, the GPP sensitivity to drought is expressed as:

$$Sens_{-p} = \frac{|\overline{GPP}_{an,-P}|}{|\bar{P}_{an,-P}|} \quad (2)$$

where $\bar{GPP}_{an,-P}$ is averaged GPP anomalies over all voxels from exclusively drought (i.e. low P) induced extreme events among the studied 1000 events; $\bar{P}_{an,-P}$ is averaged precipitation anomalies over the same voxels. Thus, $Sens_{-p}$is the sensitivity of modelled GPP to the driver, that is GPP deficit for each precipitation anomaly during extreme events.

3. Results

3.1. Spatio-temporal patterns of extreme events

Most (95%) of the GPP_{1000} had a duration of 1–7 months (Fig. A.2). To map spatial distribution of GPP anomalies, the GPP_{1000} over China were aggregated in time. In details, for a specific location, all anomalies in GPP classed as extreme events were summed and then divided by 34 years. TRENDY multi-model median showed hotspots of extreme events in North China where the GPP extreme anomalies could reach up to -70 gC m^{-2} $year^{-1}$ (Fig. 1a). In addition, regional medians of North China, Inner Mongolia and Central China had prominent GPP extreme anomalies of -53, -31 and -30 gC m^{-2} $year^{-1}$, respectively. In contrast, both Northwest China and Qinghai-Tibetan Plateau (QTP) were less impacted by extreme events with regional median GPP anomalies of approximately -10 gC m^{-2} $year^{-1}$.

According to the Yao-GPP data-driven model, the anomalies became larger in magnitude from southeast to northwest (Fig. 1b). The smallest GPP negative anomalies of less than -10 gC m^{-2} $year^{-1}$ were diagnosed in Southwest China and Sichuan Basin where there are relatively lower altitudes. The largest negative GPP extreme events were found in Inner Mongolia (-46 gC m^{-2} $year^{-1}$), Northeast China (-42 gC m^{-2} $year^{-1}$) and North China (-28 gC m^{-2} $year^{-1}$) in Yao-GPP. The prominent extreme events were generally diagnosed in mountainous regions such as Qinling Mountains in North China around Sichuan Basin, and Greater Khingan Mountains and Changbai Mountains in Northeast China. Although these regions had less GPP than South China, much more significant GPP deficits were detected. Hot spots of extreme events were detected in Northeast China for Yao-GPP but in North China for the process-based ecosystem models. Compared with Yao-GPP, the process-based ecosystem models overestimate the magnitude of extreme events in Northeast China and underestimate in North China (Fig. 1d). Disagreement among the process-based ecosystem models was mainly found in North China and South China (Fig. 1c).

The GPP_{1000} were aggregated in space to produce the monthly evolution of GPP anomalies in China, which was further aggregated to show seasonal differences (Fig. 2). The median over the TRENDY models indicated that extreme events in summer produced the most GPP negative anomalies by -30.4 TgC $month^{-1}$, which accounted for 45% anomalies of the year, followed by spring, autumn and winter.

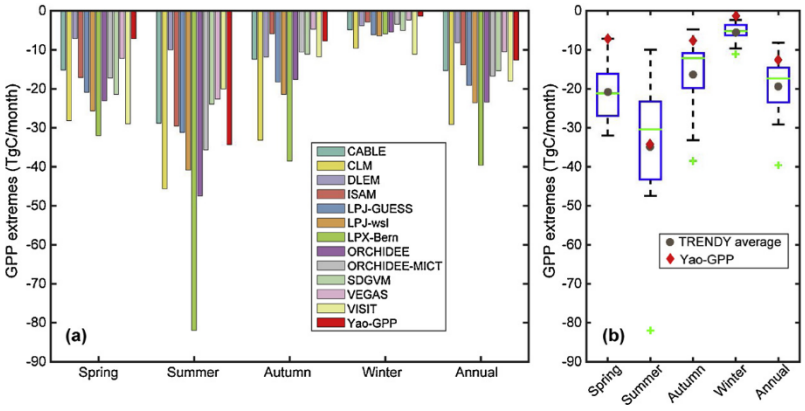

Fig. 2. (a) Bar graph and (b) boxplot of GPP extremes in four seasons and annual mean. The legend in panel (a) distinguishes the 13 GPP datasets. The red diamonds and grey dots in panel (b) represent Yao-GPP and averages over the 12 process-based models, respectively. The lower and upper edges of the box indicate 25th and 75th percentile of the GPP anomalies over the 12 process-based models. The green line and cross are median and outliers, respectively. Note that 1 TgC = 10^{12} gC.

Boxplot exhibited that LPX-Bern was an outlier in summer and autumn while VISIT was an outlier in winter over the 12 process-based models because of their overestimates of GPP deficits. The GPP deficits in Yao-GPP were smaller than the TRENDY median in spring, autumn and winter but slightly larger in summer, which consequently made the summer accounting for 68% of the mean annual anomalies in Yao-GPP. Among the 12 TRENDY models, LPX-Bern produced the largest extreme events by -475.2 TgC year^{-1} while DLEM produced the smallest extreme events by -98.4 TgC year^{-1} for the GPP_{1000} in China (Fig. A.3). The TRENDY median and Yao-GPP estimated values of -207.6 TgC year^{-1} and -151.2 TgC year^{-1} for the sum of the GPP_{1000}, accounting for 2.8% and 2.3% of mean annual GPP, respectively.

3.2. Attribution of negative GPP extremes in China and the nine sub-regions

The eight climate indices and fire variables were regarded as potential drivers of the GPP_{1000} in China. As for single climate drivers, we investigated both positive and negative anomalies in T, P, SM and scPDSI (Fig. 3a). According to the TRENDY multi-model median, both cold spell and heat wave were influential for ~26% of the extreme events. Meteorological droughts (i.e. low P) were associated with ~58% of the extreme events, making it the major driver among the nine indices. In addition, extreme events were more related to droughts than floods as low P, low scPDSI and low SM accounted for much more events than the corresponding positive values of those indices (i.e. high P, high scPDSI and high SM). But in the arguably more realistic Yao-GPP dataset, cold spell explained 36% of the extreme events, which was much larger than heat wave (18%). Drought indices were associated with less extreme negative events than wet indices, which was different from the TRENDY model results. The 10% significance threshold denotes that GPP_{1000} in Yao-GPP were nearly independent of SM, scPDSI and fire indices. As GPP extreme events are mainly driven by T and P anomalies in China at national scale, we explored the possible compound T and P effects (Fig. 3b). The GPP_{1000} from 11 out of the 13 GPP datasets were mostly associated with compound hot and drought conditions (Fig. A.4). Compound cold and wet events were also significant in both types of GPP datasets.

China has different climate zones so that the response of GPP extreme events to driver indices are expected to be different across those zones. As shown in Fig. 4, the TRENDY median indicated that extreme events in most sub-regions were mostly associated with low P, especially for North China (66%) and Inner Mongolia (62%), but not in South China (37%). In contrast, temperature extremes (i.e. cold spell or heat wave) explained more extreme events in southern China (60%–70%) than in northern China (30%–50%). For comparison with the different response to low P, the impacts of soil drought (i.e. low SM and low scPDSI) were rather stable and explained 35%–40% and 25%–30% among all sub-regions in China. In particular, low SM was associated with 42% of extreme events, followed by low P (38%) and

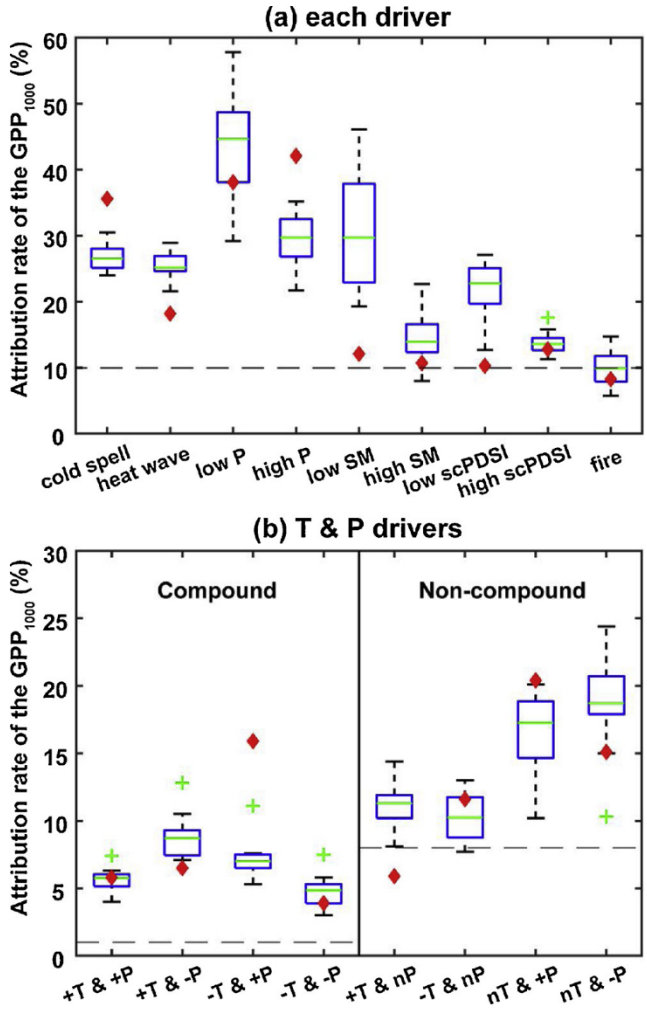

Fig. 3. Attribution rate of the GPP_{1000} for (a) each driver and (b) temperature (T) and/or precipitation (P) extremes. Boxplots result from the TRENDY models and red diamonds are for Yao-GPP. The horizontal dashed lines denote the significance threshold, below which the driver and GPP variation are expected to be independent. Notice that the threshold in panel (b) is determined by the expected attribution rate assuming the variables are independent. The nT and nP in panel (b) represent normal T (i.e. not extreme T condition) and normal P, respectively. The attribution of the GPP_{1000} in China for each model is shown in Fig. A.4.

cold spell (34%) in Southeast China. This suggested a decoupling between P and SM in controlling GPP extremes, with P anomalies combined with T anomalies enhancing evapotranspiration and decreasing

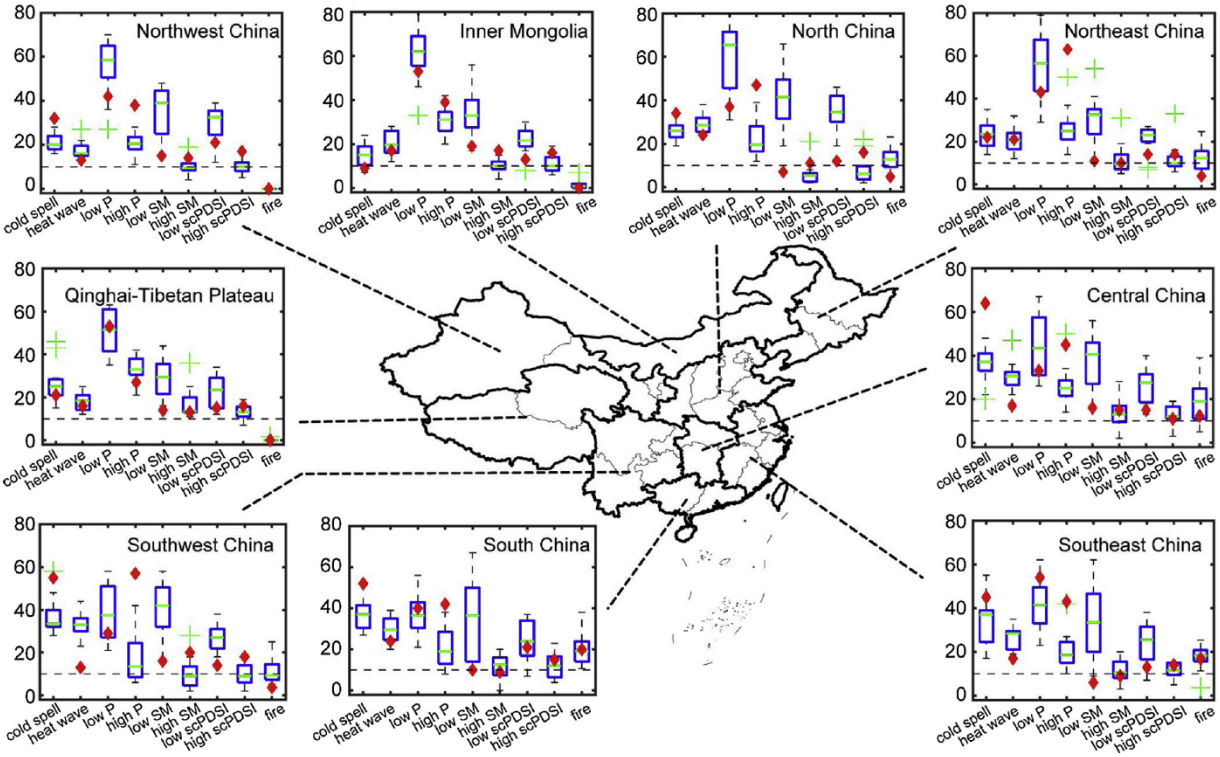

Fig. 4. Attributions rate (%) of GPP extreme events to climate drivers and fire in the nine sub-regions of China. The largest 100 negative extreme events (GPP_{100}) were used for each sub-region. Boxplots result from the TRENDY models and red diamonds are for Yao-GPP. The horizontal dashed lines denote the significance threshold (10%), below which the driver and GPP variation are expected to be independent.

SM in southern China to cause GPP extremes being more influenced by SM than by just P. The Yao-GPP also presented the different vulnerability of extreme events in GPP to temperature extremes between northern and southern China. Compared with Yao-GPP, the TRENDY models largely underestimated attribution rate for high P in most sub-regions but overestimated attribution rate for low P in northern China. For the period of 1997–2015, both Yao-GPP and TRENDY median indicated that fire was linked to 20% of large events in South China and Southeast China. In terms of compound T and P effects (Fig. A.5), we found the GPP_{100} from TRENDY were mostly associated with concurrent heat and drought events in most sub-regions of China, except in QTP. But in Yao-GPP, the result is diverse. For example, compound heat and drought events are the most important drivers in Inner Mongolia while Southwest China is more affected by concurrent cold and wet events.

3.3. Size distribution of GPP extreme events

In order to understand the characteristic of extreme events, it is crucial to know the size distribution of extreme events. The sizes of the GPP_{1000} from the 13 GPP datasets were well fitted by power law distributions (Fig. 5). The power law exponent (α-value) agreed well among the 13 datasets, ranging from 1.57 to 1.76, with the highest value in Yao-GPP and the lowest value in ORCHIDEE-MICT. The median α-value (α_m-value) over the TRENDY models was 1.68, which is slightly smaller than α-value in Yao-GPP (α_Y-value = 1.76).

It was found that different climate regions and vegetation types resulted in different α-value of fire size distribution (Hantson et al., 2015). Therefore, we supposed that size distribution of extreme events could have variations for different drivers and in sub-regions. As for the TRENDY models, the α_m had substantial fluctuation between 1.52–2.18 for different drivers (Fig. 6). The smallest α_m-value was observed for low SM (1.53, the range of 1.47–1.76 in TRENDY models) and low scPDSI (1.52, the range of 1.40–1.68 in TRENDY models) related extreme events and the largest α_m-value (2.18, the range of 2.06–3.05 in TRENDY models) was diagnosed for fire related extreme events (Table A.2). It means that low SM tended to result in large GPP negative anomalies respective to small events while fire was more associated with small sized extreme events in China. Furthermore, all α_m-values for drought induced extreme events, including meteorological drought (i.e. low P) and soil drought (i.e. low SM and low scPDSI), were significantly smaller than wet related events. Similarly, the Yao-GPP also showed that low SM (2.09) and low scPDSI (2.18) were correspondingly smaller than high SM (2.18) and high scPDSI (2.22) related events, suggesting more vulnerability of GPP to drought events than extreme wet events. Compared with α_Y-values, α_m-values were overall underestimated. Similarly, the α-values for the GPP_{100} for each sub-region in China were also diagnosed (Fig. A.6). Clear spatial decreasing gradients in α_m-values were found from the northwest to the southeast, indicating relatively more large-events were diagnosed in Southeast China (1.65) and North China (1.65).

3.4. GPP sensitivity to temperature and precipitation anomalies

The size of the extreme events is also determined by models' sensitivity. Thus, we explored the GPP sensitivities of the models to evaluate the model performance during extreme events (Fig. 7). The GPP sensitivities of Yao-GPP to heat, cold, wet and drought were 118 gC m^{-2} $month^{-1}$ $°C^{-1}$, 29 gC m^{-2} $month^{-1}$ $°C^{-1}$, 1.8 gC m^{-2} mm^{-1} and 4.1 gC m^{-2} mm^{-1}, respectively. Compared with Yao-GPP, the TRENDY median underestimated the sensitivities to heat (-18%) and drought (-42%) but overestimated the sensitivities to cold (37%) and wet (16%). Nevertheless, both TRENDY median and Yao-GPP demonstrated significantly higher GPP sensitivities to heat and drought than to cold and wet (i.e. heat/cold > 1, drought/wet > 1), highlighting the negative impacts of heat and drought events.

The GPP sensitivity to temperature or precipitation anomalies (i.e. heat, cold, wet and drought) varies significantly across the 13 models.

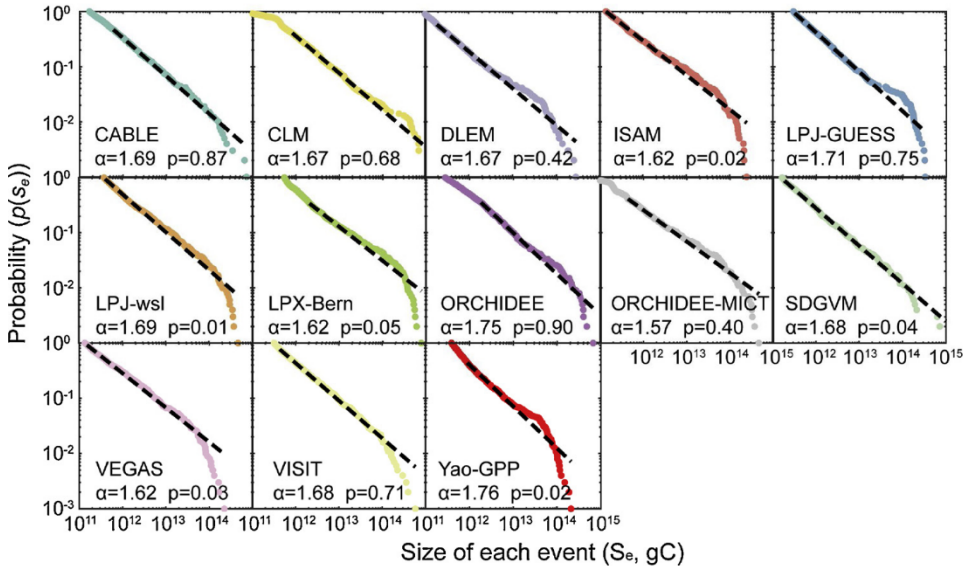

Fig. 5. Fitted power law distributions to sizes of negative GPP anomalies (gC) for the 13 GPP datasets. The letter α denotes the exponent of the fitted power law. Colored dots are the GPP_{1000} for each dataset and black dashed lines are fitted power law distribution. A p-value $\geq$ 0.1 indicates a good fit.

For example, ORCHIDEE-MICT showed the same GPP sensitivities to heat, cold as well as heat/cold ratio as Yao-GPP, but presented less response to precipitation extremes. In fact, all the process-based models except DLEM showed less sensitive to drought than Yao-GPP. TRENDY models had remarkable disagreement in heat/cold sensitivity ratio but showed better agreement in drought/wet sensitivity ratio. Nevertheless, 12 out of the 13 models were more sensitive to heat than to cold events and 10 out of the 13 models were more sensitive to drought than to wet events.

4. Discussion

The characterization of extreme events in vegetation productivity is critical for understanding its role in regulating regional carbon cycles and its climatic drivers. Our study presents the first attempt to analyze spatio-temporally contiguous GPP extreme events at the national scale and sub-regions in China. Spatial distribution of negative extreme events from Yao-GPP exhibited hotspots in Northeast China and Qinling Mountains where high interannual variability was also diagnosed in Yao et al. (2018b). Xu et al. (2012) also found that the area experiencing negative vegetation growth anomalies increased in northern China but decreased in southern China during 2000s, although the whole China experienced an increasing trend in heat waves and drought events. A strong negative NPP trend was diagnosed in Northeast China (Sitch et al., 2015), further emphasizing more concerns should be given to northern China. Based on four global GPP datasets, Zscheischler et al. (2014a) demonstrated that a few extreme events dominated global interannual variability in GPP. It could explain the similar spatial distribution between GPP negative extremes and interannual variability of GPP in most regions in China. This result highlights the importance of extreme events in regulating regional carbon cycles. In general, the effects of extreme events decreased annual GPP by 2.8% and 2.3% in TRENDY model and Yao-GPP, respectively. TRENDY median and Yao-GPP showed that extreme events in summer contributed to 45% and

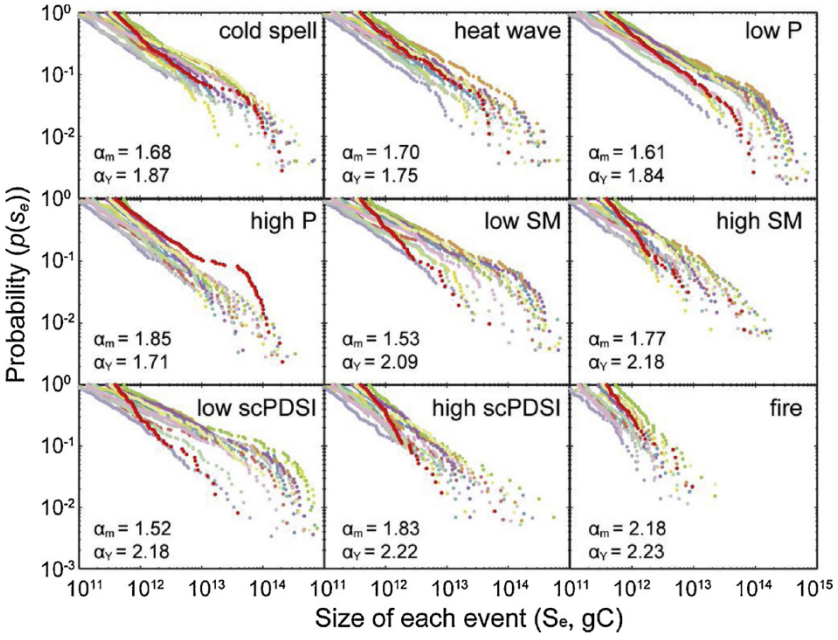

Fig. 6. Probability distributions of sizes of extreme events caused by the nine drivers, respectively. The color legend to distinguish GPP datasets is the same as in Fig. 2. Letters α_Y and α_m represent exponent for Yao-GPP and the median of the fitted exponents over the TRENDY models, respectively. The sample size, power law fitting and goodness-of-fit parameters are presented in Table A.2.

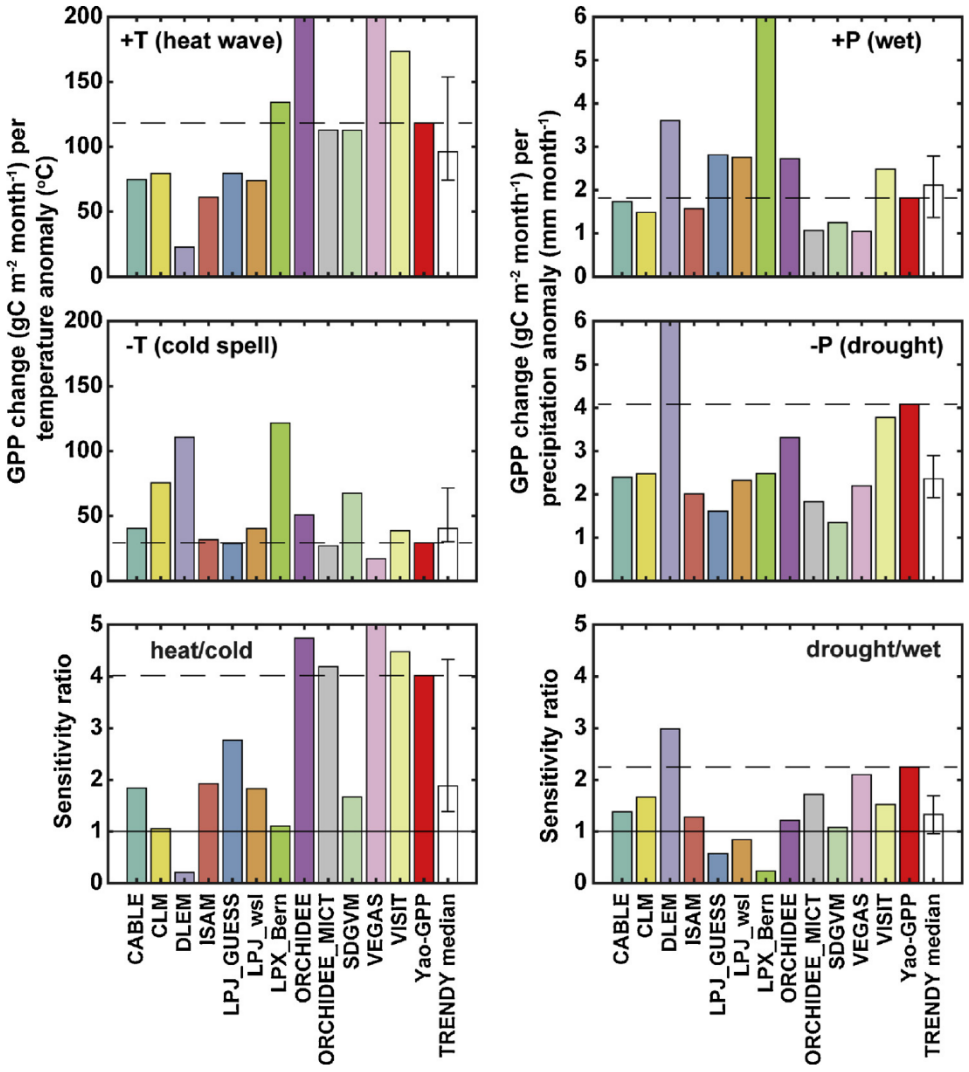

Fig. 7. Sensitivities of GPP anomalies to single driver of heat wave, cold spell, wet and drought during extreme events among the 13 models. The white bar in each panel shows TRENDY median, 25th and 75th percentile. The horizontal dashed line denotes Yao-GPP value.

68% of GPP negative anomalies, respectively, followed by spring, autumn and winter. This may be because summer usually corresponds to the highest GPP, and thus the highest absolute GPP anomalies are likely to occur when extreme events happen in summertime. For instance, in the summer of 2013, the strongest drought and heat wave on record for the past 113 years resulted in a 39–53% reduction of the annual net carbon sink of China's terrestrial ecosystems (Yuan et al., 2016).

The attribution analyses implied that low P explained 58% and 38% of the GPP_{1000} in TRENDY models and Yao-GPP, respectively. In global drought-affected areas, the reduced carbon uptake could explain larger than 70% of the interannual variation in GPP (Du et al., 2018), also emphasizing the overall significantly negative impacts of meteorological droughts on vegetation productivity. Nevertheless, the vulnerability of GPP to these nine drivers showed marked difference between northern and southern China. A few mechanisms may explain the phenomenon that droughts were associated with much more extreme events in northern China (˜60%) than in southern China (˜40%) in TRENDY models. Firstly, the different climate is partly responsible for this different response that northern China experiences annual precipitation with less than 800 mm $year^{-1}$ while southern China is moister (Fig. A.1). In addition, consecutive dry days averaged over 1961–2015 for northern China is larger than 50 days $year^{-1}$, which is much higher than southern China (Shi et al., 2018). Secondly, southern China has much higher tree density (Crowther et al., 2015), while most regions of northern China (e.g. Inner Mongolia and Northwest China) are mainly dominated by grasslands (Yao et al., 2018b). Grasslands are more susceptible to droughts in contrast to forests (Reichstein et al., 2013), probably because of shallower root system in grasslands (Teuling et al., 2010). However, compared with Yao-GPP, TRENDY models seem to overestimate the number of drought associated events (i.e. attribution rate; Fig. 3) but underestimate the GPP sensitivity to drought (Fig. 7). The over-response of GPP and leaf area index in Earth system models to droughts has previously been suggested by Huang et al. (2016). Both types of GPP datasets demonstrated that vegetation in South China is mostly vulnerable to temperature extremes, in particular cold spells. This result is consistent with results from Xu et al. (2016) and Yao et al. (2018b) that the sensitivity to temperature variability is higher in southern China, especially for forests. Compared with Yao-GPP, TRENDY models systematically underestimated cold spell-induced events and overestimated heat wave-induced events in southern China. A better representation of photosynthetic temperature acclimation in process-based models is critical to reduce the uncertainty in modeling the carbon cycle-climate feedback (Lombardozzi et al., 2015). Zscheischler et al. (2014d) highlighted the strong compound hot and dry events during 21 st century based on CMIP5 future projections. We also found the significant impacts of concurrent hot and dry events in most sub-regions of China but the GPP_{1000} were mostly associated with P anomalies during normal T for China as a whole.

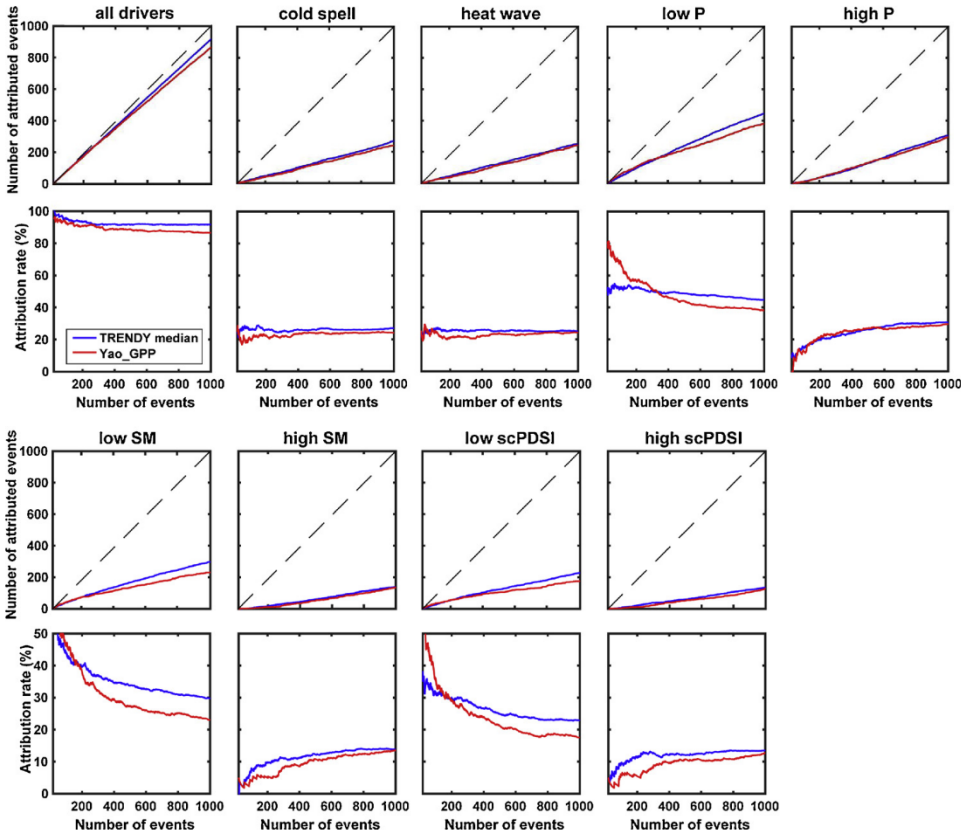

Fig. 8. Attribution rate for different number of studied largest GPP events and for each driver. The diagonal line means 1:1 line.

The power law exponent of size distributions of extreme events in China is 1.68 in TRENDY median and 1.76 in Yao-GPP, which are consistent with that in Asia (1.61) and different continental range (1.55–1.75) as extracted by Zscheischler et al. (2014c). However, the exponent varied significantly for different drivers with the range of 1.52–2.18 for TRENDY models and 1.71–2.23 in Yao-GPP (Fig. 6). In addition, the power law exponent for drought-induced extreme events were significantly smaller than for wet-related events. It means drought events are more likely to result in relatively large events while wet events provoke less GPP response. It was also supported by the plot between number of studied largest extreme events and attribution rate for P, SM and scPDSI indices (Fig. 8). When we increased the number of studied events (i.e. when looking into the smaller events), the attribution rate shows significant decreases for all drought indices but increase for all wet indices. A case study in Inner Mongolia grassland ecosystems demonstrated that both aboveground net primary productivity and CO_2 fluxes in the semiarid steppe were very stable in the face of extreme large precipitation events, regardless of the timing of the events (Hao et al., 2017). In contrast, multiyear precipitation reduction over northern China significantly decreased water availability, indicated by the Palmer Drought Severity Index and soil moisture measurements, and further resulted in strong decreases in carbon uptake (Yuan et al., 2014). Therefore, the lower sensitivity of vegetation to wet events than to droughts in our results (Fig. 7) could explain the more decisive role of droughts for negative GPP events. Based on multiple terrestrial models, Zscheischler et al. (2014b) also suggested higher drought impacts on GPP anomalies, partially during compound hot and dry conditions. The α_m-value for fire-induced extreme events is much lower than for climate drivers, implying that GPP in China is less vulnerable to fire than to climate extremes.

The on-going global warming increased extreme climate events are an increasing threat to vegetation productivity in the future (Frank et al., 2015). It has been suggested that warm extremes are more frequent and more persistent in a $+2\,^{\circ}C$ global warming scenario based on 29 climate models, especially in southern China (Sui et al., 2018). Accordingly, we could predict that southern China has to face more heat wave-induced GPP negative anomalies as it is highly vulnerable to warm extremes. The effect of cold spells in southern China is more noticeable but received less attentions than droughts. Liu et al. (2018) found that the extension of the growing season in the Northern Hemisphere may actually make plants in fact more vulnerable to frost days, which further highlights the important role of cold spell. In addition, increases in the total amount and frequency of wet extremes are projected over most regions of China, particularly in QTP (Niu et al., 2017; Sui et al., 2018), which we expect have fewer negative impacts on vegetation productivity of grasslands there. An experimental study showed that grassland plant diversity increases the resistance of ecosystem productivity to climate extremes (Isbell et al., 2015), which provides a potential strategy to face future climate extremes for a large area of grasslands in northern China. Both TRENDY models and Yao-GPP showed that less GPP deficits were observed in Sichuan basin (Fig. 1), where croplands are the dominant vegetation type, possibly implying the importance of management for mitigating damage from climate extremes. Nevertheless, we still could not rule out the damage of climate extremes on croplands as evidence also showed that droughts and heat wave episodes significantly reduced global and national crop production with a reduction in both harvested area and yields (Lesk et al., 2016; Piao et al., 2010). For instance, Lobell et al. (2012) argued that warming presented an even greater challenge to wheat than implied by previous modeling studies.

However, there are still some limitations in this study. Firstly, we have only considered time lags of a maximum of three months. There is evidence that extreme events can affect the carbon cycle concurrently and produce lagged impacts at longer time scales (e.g. through vegetation mortality) (Arnone et al., 2008; Schwalm et al., 2017). This prolonged response of vegetation GPP could be discovered in case

studies but is rather difficult to be detected by our approach. Secondly, there are ~10% of the GPP_{1000} that did not correspond to any of the nine studied factors. It is possible that extreme events may result from compound events of less extreme conditions (e.g. T and P anomalies within 10th-90th percentile). These confounding factors may have an impact on the attribution analysis, especially for small events. That may be one of the reasons why there is a slight decrease in overall attribution rate from 95% for 100 events to 92% for 1000 events in TRENDY and from 93% to 87% in Yao-GPP (Fig. 8). To perform this 3-D algorithm and to compare among models, the gridded data were interpolated to 0.1° × 0.1° spatial resolution. This processing may introduce some uncertainties at pixel scale. Finally, many factors also play important roles in regulating the vulnerability of vegetation GPP to extreme events, for instance different ecosystems (von Buttlar et al., 2018; Xu et al., 2016), management practices (He et al., 2015), and soil conditions (Nepstad et al., 2007). Thus, future studies considering more drivers and regional conditions are necessary to better understand the vulnerability and sensitivity of regional vegetation GPP to extreme events. From this, detailed management practice is possible to be carried out to mitigate the damage from future extreme events.

5. Conclusion

In this study, we investigated GPP extreme events in China and subregions based on a spatio-temporally contiguous approach using the 5th percentile definition with GPP data from 12 process-based ecosystem models and one observation-based model. Both types of models exhibited that vegetation in Northeast China and North China were most vulnerable to extreme events, especially in mountainous regions. Over the past three decades, 45% and 68% of GPP deficits in China occurred in summer in TRENDY models and Yao-GPP, respectively. Low precipitation was associated with most extreme events among the nine studied climatic drivers in China in TRENDY models. Vegetation in southern China is more vulnerable to temperature extremes (i.e. cold spell and heat wave) than in northern China. Although cold spells have received less attention than drought in previous studies, our results emphasize their potential negative impact on GPP. Both power law distribution analyses and sensitivity analysis highlight the impacts of drought on large GPP negative anomalies. Our results implied that policymakers could pay more attention to GPP deficits in northern China under drought events and in southern China under temperature extremes in order to mitigate the potential impacts of future climate extremes.

Acknowledgements

This study was supported by the Natural Science Foundation for Distinguished Young Scholars of Hubei Province of China (2016CFA051), the National Natural Science Foundation of China (No. 41772029 and 41322013), the 111 Project (No. B14031 and B08030). W. Chen acknowledges support from the China Scholarship Council (No. 201806410044) for Ph.D. work at LSCE, France. S. Lienert acknowledges support from the Swiss National Science Foundation (No. 20020_172476).

Appendix A. Supplementary data

Supplementary material related to this article can be found, in the online version, at doi:https://doi.org/10.1016/j.agrformet.2019.05.002.

References

Arnone 3rd, J.A., Verburg, P.S., Johnson, D.W., Larsen, J.D., Jasoni, R.L., Lucchesi, A.J., Batts, C.M., von Nagy, C., Coulombe, W.G., Schorran, D.E., Buck, P.E., Braswell, B.H., Coleman, J.S., Sherry, R.A., Wallace, L.L., Luo, Y., Schimel, D.S., 2008. Prolonged suppression of ecosystem carbon dioxide uptake after an anomalously warm year. Nature 455 (7211), 383–386.

Chen, Y., Yang, K., He, J., Qin, J., Shi, J., Du, J., He, Q., 2011. Improving land surface temperature modeling for dry land of China. J. Geophys. Res. Atmos. 116 D20104.

Chen, W., Huang, C., Wang, L., Li, D., 2018. Climate extremes and their impacts on interannual vegetation variabilities: a case study in Hubei Province of Central China. Remote Sens. 10 (3), 477.

Ciais, P., Reichstein, M., Viovy, N., Granier, A., Ogee, J., Allard, V., Aubinet, M., Buchmann, N., Bernhofer, C., Carrara, A., Chevallier, F., De Noblet, N., Friend, A.D., Friedlingstein, P., Grunwald, T., Heinesch, B., Keronen, P., Knohl, A., Krinner, G., Loustau, D., Manca, G., Matteucci, G., Miglietta, F., Ourcival, J.M., Papale, D., Pilegaard, K., Rambal, S., Seufert, G., Soussana, J.F., Sanz, M.J., Schulze, E.D., Vesala, T., Valentini, R., 2005. Europe-wide reduction in primary productivity caused by the heat and drought in 2003. Nature 437 (7058), 529–533.

Clauset, A., Shalizi, C.R., Newman, M.E.J., 2009. Power-law distributions in empirical data. SIAM Rev. Soc. Ind. Appl. Math. 51 (4), 661–703.

Crowther, T.W., Glick, H.B., Covey, K.R., Bettigole, C., Maynard, D.S., Thomas, S.M., Smith, J.R., Hintler, G., Duguid, M.C., Amatulli, G., Tuanmu, M.N., Jetz, W., Salas, C., Stam, C., Piotto, D., Tavani, R., Green, S., Bruce, G., Williams, S.J., Wiser, S.K., Huber, M.O., Hengeveld, G.M., Nabuurs, G.J., Tikhonova, E., Borchardt, P., Li, C.F., Powrie, L.W., Fischer, M., Hemp, A., Homeier, J., Cho, P., Vibrans, A.C., Umunay, P.M., Piao, S.L., Rowe, C.W., Ashton, M.S., Crane, P.R., Bradford, M.A., 2015. Mapping tree density at a global scale. Nature 525 (7568), 201–205.

Cui, L., Wang, L., Singh, R.P., Lai, Z., Jiang, L., Yao, R., 2018. Association analysis between spatiotemporal variation of vegetation greenness and precipitation/temperature in the Yangtze River Basin (China). Environ. Sci. Pollut. Res. 1–12.

Du, L., Mikle, N., Zou, Z., Huang, Y., Shi, Z., Jiang, L., McCarthy, H.R., Liang, J., Luo, Y., 2018. Global patterns of extreme drought-induced loss in land primary production: identifying ecological extremes from rain-use efficiency. Sci. Total Environ. 628-629, 611–620.

Felton, A.J., Smith, M.D., 2017. Integrating plant ecological responses to climate extremes from individual to ecosystem levels. Philos. Trans. R. Soc. Lond., B Biol. Sci. 372, 1723.

Frank, D., Reichstein, M., Bahn, M., Thonicke, K., Frank, D., Mahecha, M.D., Smith, P., van der Velde, M., Vicca, S., Babst, F., Beer, C., Buchmann, N., Canadell, J.G., Ciais, P., Cramer, W., Ibrom, A., Miglietta, F., Poulter, B., Rammig, A., Seneviratne, S.I., Walz, A., Wattenbach, M., Zavala, M.A., Zscheischler, J., 2015. Effects of climate extremes on the terrestrial carbon cycle: concepts, processes and potential future impacts. Glob. Chang. Biol. 21 (8), 2861–2880.

Ge, J., Xiong, G., Wang, Z., Zhang, M., Zhao, C., Shen, G., Xu, W., Xie, Z., 2015. Altered dynamics of broad-leaved tree species in a Chinese subtropical montane mixed forest: the role of an anomalous extreme 2008 ice storm episode. Ecol. Evol. 5 (7), 1484–1493.

Guimberteau, M., Zhu, D., Maignan, F., Huang, Y., Yue, C., Dantec-Nédélec, S., Ottlé, C., Jornet-Puig, A., Bastos, A., Laurent, P., Goll, D., Bowring, S., Chang, J., Guenet, B., Tifafi, M., Peng, S., Krinner, G., Ducharne, A., Wang, F., Wang, T., Wang, X., Wang, Y., Yin, Z., Lauerwald, R., Joetzjer, E., Qiu, C., Kim, H., Ciais, P., 2018. ORCHIDEE-MICT (v8.4.1), a land surface model for the high latitudes: model description and validation. Geosci. Model. Dev. Discuss. 11 (1), 121–163.

Hantson, S., Pueyo, S., Chuvieco, E., 2015. Global fire size distribution is driven by human impact and climate. Global Ecol. Biogeogr. 24 (1), 77–86.

Hao, Y.B., Zhou, C.T., Liu, W.J., Li, L.F., Kang, X.M., Jiang, L.L., Cui, X.Y., Wang, Y.F., Zhou, X.Q., Xu, C.Y., 2017. Aboveground net primary productivity and carbon balance remain stable under extreme precipitation events in a semiarid steppe ecosystem. Agric. For. Meteorol. 240-241, 1–9.

Harris, I., Jones, P., Osborn, T., Lister, D., 2014. Updated high-resolution grids of monthly climatic observations–the CRU TS3. 10 Dataset. Int. J. Climatol. 34 (3), 623–642.

Haverd, V., Smith, B., Nieradzik, L., Briggs, P.R., Woodgate, W., Trudinger, C.M., Canadell, J.G., Cuntz, M., 2018. A new version of the CABLE land surface model (Subversion revision r4601) incorporating land use and land cover change, woody vegetation demography, and a novel optimisation-based approach to plant coordination of photosynthesis. Geosci. Model. Dev. Discuss. 11 (7), 2995–3026.

He, S., Richards, K., Zhao, Z., 2015. Climate extremes in the Kobresia meadow area of the Qinghai-Tibetan Plateau, 1961–2008. Environ. Earth Sci. 75 (1), 15.

Huang, Y., Gerber, S., Huang, T., Lichstein, J.W., 2016. Evaluating the drought response of CMIP5 models using global gross primary productivity, leaf area, precipitation, and soil moisture data. Global Biogeochem. Cycles 30 (12), 1827–1846.

IPCC, 2012. Managing the Risks of Extreme Events and Disasters to Advance Climate Change Adaption. Cambridge University Press, Cambridge, UK.

IPCC, 2013. Climate Change 2013: The Physical Science Basis. Contribution of Working Group I to the Fifth Assessment Report of the Intergovernmental Panel on Climate Change. Cambridge University Press, Cambridge, UK, New York, NY, USA.

Isbell, F., Craven, D., Connolly, J., Loreau, M., Schmid, B., Beierkuhnlein, C., Bezemer, T.M., Bonin, C., Bruelheide, H., de Luca, E., Ebeling, A., Griffin, J.N., Guo, Q., Hautier, Y., Hector, A., Jentsch, A., Kreyling, J., Lanta, V., Manning, P., Meyer, S.T., Mori, A.S., Naeem, S., Niklaus, P.A., Polley, H.W., Reich, P.B., Roscher, C., Seabloom, E.W., Smith, M.D., Thakur, M.P., Tilman, D., Tracy, B.F., van der Putten, W.H., van Ruijven, J., Weigelt, A., Weisser, W.W., Wilsey, B., Eisenhauer, N., 2015. Biodiversity increases the resistance of ecosystem productivity to climate extremes. Nature 526 (7574), 574–577.

Jain, A.K., Meiyappan, P., Song, Y., House, J.I., 2013. CO2 emissions from land-use change affected more by nitrogen cycle, than by the choice of land-cover data. Glob. Chang. Biol. 19 (9), 2893–2906.

Jung, M., Reichstein, M., Margolis, H.A., Cescatti, A., Richardson, A.D., Arain, M.A., Arneth, A., Bernhofer, C., Bonal, D., Chen, J., 2011. Global patterns of land-atmosphere fluxes of carbon dioxide, latent heat, and sensible heat derived from eddy

covariance, satellite, and meteorological observations. J. Geophys. Res. 116 (G3), 245–255.
Kato, E., Kinoshita, T., Ito, A., Kawamiya, M., Yamagata, Y., 2013. Evaluation of spatially explicit emission scenario of land-use change and biomass burning using a process-based biogeochemical model. J. Land Use Sci. 8 (1), 104–122.
Keller, K.M., Lienert, S., Bozbiyik, A., Stocker, T.F., Churakova, O.V., Frank, D.C., Klesse, S., Koven, C.D., Leuenberger, M., Riley, W.J., Saurer, M., Siegwolf, R., Weigt, R.B., Joos, F., 2017. 20th century changes in carbon isotopes and water-use efficiency: tree-ring-based evaluation of the CLM4.5 and LPX-Bern models. Biogeosciences 14 (10), 2641–2673.
Krinner, G., Viovy, N., de Noblet-Ducoudré, N., Ogée, J., Polcher, J., Friedlingstein, P., Ciais, P., Sitch, S., Prentice, I.C., 2005. A dynamic global vegetation model for studies of the coupled atmosphere-biosphere system. Global Biogeochem. Cycles 19 (1).
Le Quéré, C., Andrew, R.M., Friedlingstein, P., Sitch, S., Pongratz, J., Manning, A.C., Korsbakken, J.I., Peters, G.P., Canadell, J.G., Jackson, R.B., Boden, T.A., Tans, P.P., Andrews, O.D., Arora, V.K., Bakker, D.C.E., Barbero, L., Becker, M., Betts, R.A., Bopp, L., Chevallier, F., Chini, L.P., Ciais, P., Cosca, C.E., Cross, J., Currie, K., Gasser, T., Harris, I., Hauck, J., Haverd, V., Houghton, R.A., Hunt, C.W., Hurtt, G., Ilyina, T., Jain, A.K., Kato, E., Kautz, M., Keeling, R.F., Klein Goldewijk, K., Körtzinger, A., Landschützer, P., Lefèvre, N., Lenton, A., Lienert, S., Lima, I., Lombardozzi, D., Metzl, N., Millero, F., Monteiro, P.M.S., Munro, D.R., Nabel, J.E.M.S., Nakaoka, S.-i., Nojiri, Y., Padin, X.A., Peregon, A., Pfeil, B., Pierrot, D., Poulter, B., Rehder, G., Reimer, J., Rödenbeck, C., Schwinger, J., Séférian, R., Skjelvan, I., Stocker, B.D., Tian, H., Tilbrook, B., Tubiello, F.N., van der Laan-Luijkx, I.T., van der Werf, G.R., van Heuven, S., Viovy, N., Vuichard, N., Walker, A.P., Watson, A.J., Wiltshire, A.J., Zaehle, S., Zhu, D., 2018. Global carbon budget 2017. Earth Syst. Sci. Data Discuss. 10 (1), 405–448.
Lesk, C., Rowhani, P., Ramankutty, N., 2016. Influence of extreme weather disasters on global crop production. Nature 529 (7584), 84–87.
Liu, Q., Piao, S., Janssens, I.A., Fu, Y., Peng, S., Lian, X., Ciais, P., Myneni, R.B., Penuelas, J., Wang, T., 2018. Extension of the growing season increases vegetation exposure to frost. Nat. Commun. 9 (1), 426.
Lloyd-Hughes, B., 2012. A spatio-temporal structure-based approach to drought characterisation. Int. J. Climatol. 32 (3), 406–418.
Lobell, D.B., Sibley, A., Ivan Ortiz-Monasterio, J., 2012. Extreme heat effects on wheat senescence in India. Nat. Clim. Change 2 (3), 186–189.
Lombardozzi, D.L., Bonan, G.B., Smith, N.G., Dukes, J.S., Fisher, R.A., 2015. Temperature acclimation of photosynthesis and respiration: a key uncertainty in the carbon cycle-climate feedback. Geophys. Res. Lett. 42 (20), 8624–8631.
Los, S.O., 2013. Analysis of trends in fused AVHRR and MODIS NDVI data for 1982–2006: indication for a CO2 fertilization effect in global vegetation. Global Biogeochem. Cycles 27 (2), 318–330.
Nepstad, D.C., Tohver, I.M., Ray, D., Moutinho, P., Cardinot, G., 2007. Mortality of large trees and lianas following experimental drought in an Amazon forest. Ecology 88 (9), 2259–2269.
Niu, X., Wang, S., Tang, J., Lee, D.K., Gutowski, W., Dairaku, K., McGregor, J., Katzfey, J., Gao, X., Wu, J., 2017. Ensemble evaluation and projection of climate extremes in China using RMIP models. Int. J. Climatol. 38 (4), 2039–2055.
Oleson, K., Lawrence, M., Bonan, B., Drewniak, B., Huang, M., Koven, D., Levis, S., Li, F., Riley, J., Subin, M., 2013. Technical Description of Version 4.5 of the Community Land Model (CLM).
Piao, S., Ciais, P., Huang, Y., Shen, Z., Peng, S., Li, J., Zhou, L., Liu, H., Ma, Y., Ding, Y., Friedlingstein, P., Liu, C., Tan, K., Yu, Y., Zhang, T., Fang, J., 2010. The impacts of climate change on water resources and agriculture in China. Nature 467 (7311), 43–51.
Piao, S., Sitch, S., Ciais, P., Friedlingstein, P., Peylin, P., Wang, X., Ahlstrom, A., Anav, A., Canadell, J.G., Cong, N., Huntingford, C., Jung, M., Levis, S., Levy, P.E., Li, J., Lin, X., Lomas, M.R., Lu, M., Luo, Y., Ma, Y., Myneni, R.B., Poulter, B., Sun, Z., Wang, T., Viovy, N., Zaehle, S., Zeng, N., 2013. Evaluation of terrestrial carbon cycle models for their response to climate variability and to CO2 trends. Glob. Chang. Biol. 19 (7), 2117–2132.
Randerson, J.T., van der Werf, G.R., Giglio, L., Collatz, G.J., Kasibhatla, P.S., 2017. Global Fire Emissions Database, Version 4.1 (GFEDv4). Global Fire Emissions Database, Version 4.1 (GFEDv4). ORNL DAAC, Oak Ridge, Tennessee, USA.
Reichstein, M., Bahn, M., Ciais, P., Frank, D., Mahecha, M.D., Seneviratne, S.I., Zscheischler, J., Beer, C., Buchmann, N., Frank, D.C., Papale, D., Rammig, A., Smith, P., Thonicke, K., van der Velde, M., Vicca, S., Walz, A., Wattenbach, M., 2013. Climate extremes and the carbon cycle. Nature 500 (7462), 287–295.
Ren, W., Tian, H., Tao, B., Huang, Y., Pan, S., 2012. China's crop productivity and soil carbon storage as influenced by multifactor global change. Glob. Chang. Biol. 18 (9), 2945–2957.
Samaniego, L., Thober, S., Kumar, R., Wanders, N., Rakovec, O., Pan, M., Zink, M., Sheffield, J., Wood, E.F., Marx, A., 2018. Anthropogenic warming exacerbates European soil moisture droughts. Nat. Clim. Change 8 (5), 421–426.
Scannell, H.A., Pershing, A.J., Alexander, M.A., Thomas, A.C., Mills, K.E., 2016. Frequency of marine heatwaves in the North Atlantic and North Pacific since 1950. Geophys. Res. Lett. 43 (5), 2069–2076.
Schwalm, C.R., Anderegg, W.R.L., Michalak, A.M., Fisher, J.B., Biondi, F., Koch, G., Litvak, M., Ogle, K., Shaw, J.D., Wolf, A., Huntzinger, D.N., Schaefer, K., Cook, R., Wei, Y., Fang, Y., Hayes, D., Huang, M., Jain, A., Tian, H., 2017. Global patterns of drought recovery. Nature 548 (7666), 202–205.
Shi, J., Cui, L., Wen, K., Tian, Z., Wei, P., Zhang, B., 2018. Trends in the consecutive days of temperature and precipitation extremes in China during 1961-2015. Environ. Res. 161, 381–391.
Sitch, S., Smith, B., Prentice, I.C., Arneth, A., Bondeau, A., Cramer, W., Kaplan, J.O., Levis, S., Lucht, W., Sykes, M.T., Thonicke, K., Venevsky, S., 2003. Evaluation of ecosystem dynamics, plant geography and terrestrial carbon cycling in the LPJ dynamic global vegetation model. Glob. Change Biol. Bioenergy 9 (2), 161–185.
Sitch, S., Friedlingstein, P., Gruber, N., Jones, S.D., Murray-Tortarolo, G., Ahlström, A., Doney, S.C., Graven, H., Heinze, C., Huntingford, C., Levis, S., Levy, P.E., Lomas, M., Poulter, B., Viovy, N., Zaehle, S., Zeng, N., Arneth, A., Bonan, G., Bopp, L., Canadell, J.G., Chevallier, F., Ciais, P., Ellis, R., Gloor, M., Peylin, P., Piao, S.L., Le Quéré, C., Smith, B., Zhu, Z., Myneni, R., 2015. Recent trends and drivers of regional sources and sinks of carbon dioxide. Biogeosciences 12 (3), 653–679.
Smith, B., Wårlind, D., Arneth, A., Hickler, T., Leadley, P., Siltberg, J., Zaehle, S., 2014. Implications of incorporating N cycling and N limitations on primary production in an individual-based dynamic vegetation model. Biogeosciences 11 (7), 2027–2054.
Sui, Y., Lang, X., Jiang, D., 2018. Projected signals in climate extremes over China associated with a 2 °C global warming under two RCP scenarios. Int. J. Climatol. 38 (S1), e678–e697.
Teuling, A.J., Seneviratne, S.I., Stöckli, R., Reichstein, M., Moors, E., Ciais, P., Luyssaert, S., van den Hurk, B., Ammann, C., Bernhofer, C., Dellwik, E., Gianelle, D., Gielen, B., Grünwald, T., Klumpp, K., Montagnani, L., Moureaux, C., Sottocornola, M., Wohlfahrt, G., 2010. Contrasting response of European forest and grassland energy exchange to heatwaves. Nat. Geosci. 3 (10), 722–727.
Tian, H., Chen, G., Lu, C., Xu, X., Hayes, D.J., Ren, W., Pan, S., Huntzinger, D.N., Wofsy, S.C., 2015. North American terrestrial CO2 uptake largely offset by CH4 and N2O emissions: toward a full accounting of the greenhouse gas budget. Clim. Change 129 (3-4), 413–426.
Tian, H., Ren, W., Tao, B., Sun, G., Chappelka, A., Wang, X., Pan, S., Yang, J., Liu, J., Felzer, S., 2016. Climate extremes and ozone pollution: a growing threat to China's food security. Ecosyst. Health Sustain. 2 (1) e01203.
van der Schrier, G., Barichivich, J., Briffa, K.R., Jones, P.D., 2013. A scPDSI-based global data set of dry and wet spells for 1901-2009. J. Geophys. Res. Atmos. 118 (10), 4025–4048.
von Buttlar, J., Zscheischler, J., Rammig, A., Sippel, S., Reichstein, M., Knohl, A., Jung, M., Menzer, O., Arain, M.A., Buchmann, N., Cescatti, A., Gianelle, D., Kiely, G., Law, B.E., Magliulo, V., Margolis, H., McCaughey, H., Merbold, L., Migliavacca, M., Montagnani, L., Oechel, W., Pavelka, M., Peichl, M., Rambal, S., Raschi, A., Scott, R.L., Vaccari, F.P., van Gorsel, E., Varlagin, A., Wohlfahrt, G., Mahecha, M.D., 2018. Impacts of droughts and extreme-temperature events on gross primary production and ecosystem respiration: a systematic assessment across ecosystems and climate zones. Biogeosciences 15 (5), 1293–1318.
Wang, L., Zhu, H., Lin, A., Zou, L., Qin, W., Du, Q., 2017. Evaluation of the latest MODIS GPP products across multiple biomes using global eddy covariance flux data. Remote Sens. 9 (5), 418.
Woodward, F.I., Smith, T.M., Emanuel, W.R., 1995. A global land primary productivity and phytogeography model. Global Biogeochem. Cycles 9 (4), 471–490.
Xu, X., Piao, S., Wang, X., Chen, A., Ciais, P., Myneni, R.B., 2012. Spatio-temporal patterns of the area experiencing negative vegetation growth anomalies in China over the last three decades. Environ. Res. Lett. 7 (3), 9.
Xu, Y., Shen, Z.-H., Ying, L.-X., Ciais, P., Liu, H.-Y., Piao, S.-l., Wen, C., Jiang, Y.-X., 2016. The exposure, sensitivity and vulnerability of natural vegetation in China to climate thermal variability (1901–2013): an indicator-based approach. Ecol. Indic. 63, 258–272.
Yao, J., Chen, Y., Zhao, Y., Mao, W., Xu, X., Liu, Y., Yang, Q., 2018a. Response of vegetation NDVI to climatic extremes in the arid region of Central Asia: a case study in Xinjiang. China. Theor. Appl. Climatol. 131, 1503–1515.
Yao, Y., Wang, X., Li, Y., Wang, T., Shen, M., Du, M., He, H., Li, Y., Luo, W., Ma, M., Ma, Y., Tang, Y., Wang, H., Zhang, X., Zhang, Y., Zhao, L., Zhou, G., Piao, S., 2018b. Spatiotemporal pattern of gross primary productivity and its covariation with climate in China over the last thirty years. Glob. Chang. Biol. 24 (1), 184–196.
Yao, R., Wang, L., Huang, X., Chen, X., Liu, Z., 2019. Increased spatial heterogeneity in vegetation greenness due to vegetation greening in mainland China. Ecol. Indic. 99, 240–250.
Yuan, W., Liu, D., Dong, W., Liu, S., Zhou, G., Yu, G., Zhao, T., Feng, J., Ma, Z., Chen, J., Chen, Y., Chen, S., Han, S., Huang, J., Li, L., Liu, H., Liu, S., Ma, M., Wang, Y., Xia, J., Xu, W., Zhang, Q., Zhao, X., Zhao, L., 2014. Multiyear precipitation reduction strongly decreases carbon uptake over northern China. J. Geophys. Res. Biogeosci. 119 (5), 881–896.
Yuan, W., Cai, W., Chen, Y., Liu, S., Dong, W., Zhang, H., Yu, G., Chen, Z., He, H., Guo, W., Liu, D., Liu, S., Xiang, W., Xie, Z., Zhao, Z., Zhou, G., 2016. Severe summer heatwave and drought strongly reduced carbon uptake in Southern China. Sci. Rep. 6, 18813.
Zeng, N., Mariotti, A., Wetzel, P., 2005. Terrestrial mechanisms of interannual CO(2) variability. Global Biogeochem. Cycles 19 (1).
Zhang, L., Xiao, J., Li, J., Wang, K., Lei, L., Guo, H., 2012. The 2010 spring drought reduced primary productivity in southwestern China. Environ. Res. Lett. 7 (4), 045706.
Zhou, G., Wei, X., Chen, X., Zhou, P., Liu, X., Xiao, Y., Sun, G., Scott, D.F., Zhou, S., Han, L., Su, Y., 2015. Global pattern for the effect of climate and land cover on water yield. Nat. Commun. 6 (3), 5918.
Zhu, Z., Piao, S., Myneni, R.B., Huang, M., Zeng, Z., Canadell, J.G., Ciais, P., Sitch, S., Friedlingstein, P., Arneth, A., Cao, C., Cheng, L., Kato, E., Koven, C., Li, Y., Lian, X., Liu, Y., Liu, R., Mao, J., Pan, Y., Peng, S., Peñuelas, J., Poulter, B., Pugh, T.A.M., Stocker, B.D., Viovy, N., Wang, X., Wang, Y., Xiao, Z., Yang, H., Zaehle, S., Zeng, N., 2016. Greening of the Earth and its drivers. Nat. Clim. Change 6 (8), 791–795.
Zscheischler, J., Mahecha, M.D., Harmeling, S., Reichstein, M., 2013. Detection and attribution of large spatiotemporal extreme events in Earth observation data. Pediatr. Adolesc. Gynecol. 15, 66–73.
Zscheischler, J., Mahecha, M.D., von Buttlar, J., Harmeling, S., Jung, M., Rammig, A., Randerson, J.T., Schölkopf, B., Seneviratne, S.I., Tomelleri, E., Zaehle, S., Reichstein,

M., 2014a. A few extreme events dominate global interannual variability in gross primary production. Environ. Res. Lett. 9 (3), 035001.
Zscheischler, J., Michalak, A.M., Schwalm, C., Mahecha, M.D., Huntzinger, D.N., Reichstein, M., Berthier, G., Ciais, P., Cook, R.B., El-Masri, B., Huang, M., Ito, A., Jain, A., King, A., Lei, H., Lu, C., Mao, J., Peng, S., Poulter, B., Ricciuto, D., Shi, X., Tao, B., Tian, H., Viovy, N., Wang, W., Wei, Y., Yang, J., Zeng, N., 2014b. Impact of large-scale climate extremes on biospheric carbon fluxes: An intercomparison based on MsTMIP data. Global Biogeochem. Cycles 28 (6), 585–600.
Zscheischler, J., Reichstein, M., Harmeling, S., Rammig, A., Tomelleri, E., Mahecha, M.D., 2014c. Extreme events in gross primary production: a characterization across continents. Biogeosciences 11 (11), 2909–2924.
Zscheischler, J., Reichstein, M., von Buttlar, J., Mu, M., Randerson, J.T., Mahecha, M.D., 2014d. Carbon cycle extremes during the 21st century in CMIP5 models: future evolution and attribution to climatic drivers. Geophys. Res. Lett. 41 (24), 8853–8861.
Zscheischler, J., Westra, S., van den Hurk, B.J.J.M., Seneviratne, S.I., Ward, P.J., Pitman, A., AghaKouchak, A., Bresch, D.N., Leonard, M., Wahl, T., Zhang, X., 2018. Future climate risk from compound events. Nat. Clim. Change 8 (6), 469–477.